

# Physical properties of Taurid meteoroids of various sizes

Jiří Borovička and Pavel Spurný

*Astronomical Institute of the Czech Academy of Sciences, Fričova 298, CZ-25165  
Ondřejov, Czech Republic*

---

## Abstract

The origin of the Taurid complex is still debated. In addition to comet 2P/Encke, various asteroids were proposed to be members of the complex and thus possible parent bodies of Taurid meteoroids. Studies of physical properties of Taurid meteoroids can provide constraints on their source. We used a well defined orbital sample of 16 Taurid fireballs with detailed radiometric light curves. The sample represented meteoroids of initial masses from 8 grams to 650 kg (diameters 1 – 70 cm). The semi-empirical fragmentation model was used to study their atmospheric fragmentation and derive strength distribution within the meteoroids. It was found that small meteoroids are stronger than large ones. When considering Taurid material as a whole, the majority has a very low strength of less than 0.01 MPa and a density less than  $1000 \text{ kg m}^{-3}$ . The low strength material exists mostly as large bodies ( $> 10 \text{ cm}$ ). If encountered in smaller bodies, it forms only a minor part. Stronger materials up to 0.3 MPa exist in Taurids as well, but the stronger material the rarer it is. Strong material forms small inclusions in large bodies or exists as small (cm-sized) separate bodies. These properties strongly suggest cometary origin of Taurids.

*Keywords:*

meteors, meteoroids, Taurids, comets, 2P/Encke, asteroids

---

## 1. Introduction

Taurids is an annual meteor shower characterized by a low but long activity, lasting for more than two months (Jenniskens, 2006). Taurid meteoroids have short orbital periods of about 3.4 years and low inclinations. The comet with the shortest period, 2P/Encke, is a plausible parent body but it was proposed that 2P/Encke is just one fragment of a much larger comet, which

disrupted tens of thousands years ago (Clube and Napier, 1984) and formed a whole complex. A number of asteroids was proposed to be members of the Taurid complex and thus parent bodies of Taurid meteoroids (see Kasuga and Jewitt, 2019, and references therein).

In some years, Taurid activity is enhanced and the shower is rich in fireballs. It was proposed that the enhanced activity is caused by a swarm of meteoroids trapped in the 7:2 resonance with Jupiter (Asher and Clube, 1993). Spurný et al. (2017) proved that the enhanced activity in 2015 was caused by a well-defined orbital structure, with meteoroids indeed being in the 7:2 resonance. This structure, called the new branch, was unexpectedly active also in 2018 (Spurný and Borovička, 2019), meaning that the resonant swarm is more extended than supposed by Asher and Clube (1993).

This paper is devoted to physical properties of Taurid meteoroids. The knowledge of physical properties is important for understanding the origin of the Taurid complex. There is also non-negligible impact risk with members of the Taurid complex. The new branch, which intersects the Earth’s orbit, contains also asteroids of sizes of the order of 100 m (Spurný et al., 2017). Understanding the structure of Taurid material can help to evaluate potential consequences of collision with such a large body.

Physical studies of Taurids performed so far gave mixed results. The estimates of bulk densities are dependent on the used model and vary from  $400 \text{ kg m}^{-3}$  (Bellot Rubio et al., 2002) or  $1600 \text{ kg m}^{-3}$  (Babadzhanov and Kokhirova, 2009) to  $2300 - 2800 \text{ kg m}^{-3}$  (Kononova, 2003). Kononova (2003) studied Taurid atmospheric fragmentation events in detail and found them to occur under dynamic pressures of  $0.05 - 0.18 \text{ MPa}$ . She also found significant lateral velocities of fragments and concluded that fragmentations are explosive events. Matlovič et al. (2017) found Taurids to be a heterogeneous population of meteoroids, which are cometary in nature but contain solid, possibly carbonaceous inclusions. The derived *mineralogical* densities varied from  $1300$  to  $2500 \text{ kg m}^{-3}$  (bulk densities are expected to be lower due to a porosity). Fragmentation strengths were in the range  $0.02 - 0.10 \text{ MPa}$ .

Since the orbits of Taurids fall in the region occupied by many Near Earth Asteroids, studies of Taurids can be affected by contamination of meteoroids with different origin. Both Brown et al. (2013) and Madieto et al. (2014) reported Taurid fireballs which possibly dropped meteorites and were therefore quite strong. However, the orbits of those fireballs suggest that they may not belong to Taurids at all. Here we study 16 Taurids for which there is no doubt that they really belong to the shower: 15 of them were members of

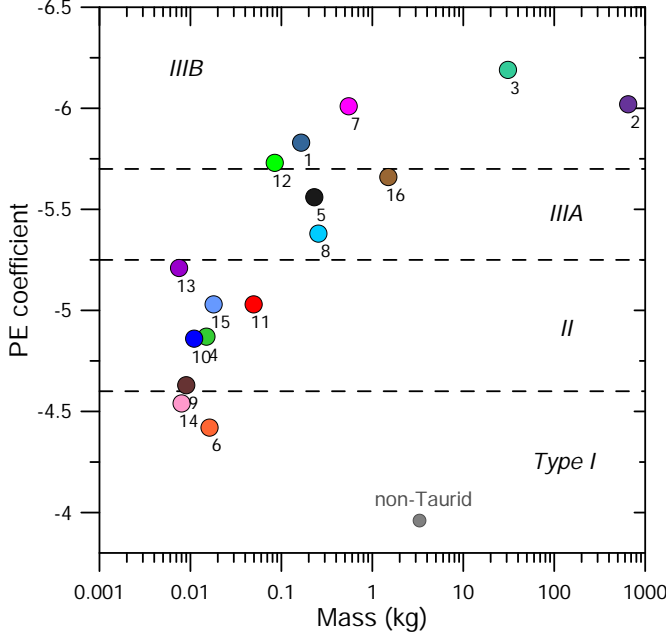


Figure 1: PE coefficient as a function of mass for Taurid fireballs studied here. For fireball numbers see Table 1. One non-Taurid was added for comparison. Fireball type according to the PE coefficient is indicated.

the well-defined new branch (14 were observed in 2015 and one in 2018), one was a regular Southern Taurid. Our sample contains meteoroids of masses covering five orders of magnitude: from  $10^{-2}$  kg to almost  $10^3$  kg. Spurný et al. (2017) already noted that the largest meteoroids belong to the most fragile type IIIB when classified according to the PE criterion (comparing end height with initial mass and speed and trajectory slope) of Ceplecha and McCrosky (1976), while small meteoroids belong to type II and some of them even to the strongest type I. In this paper we want to shed light on this interesting pattern by detailed fragmentation modeling.

## 2. Data and methods

### 2.1. Instrumentation

The data analyzed here were obtained by the Digital Autonomous Fireball Observatories (DAFO) in the scope of the European Fireball Network.

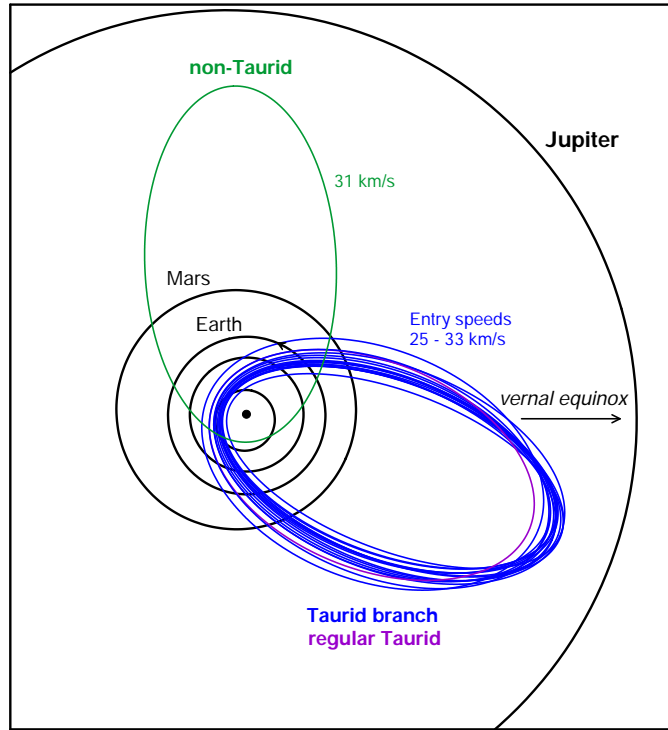


Figure 2: Orbits of studied Taurids and one non-Taurid used for comparison.

The observatories have been introduced in Spurný et al. (2017). They provide digital all-sky images and radiometric light curves of fireballs. Fireball trajectories, velocities, decelerations, and orbits are computed from multi-station photographs. Velocity measurements are enabled by a LCD shutter interrupting the 35 s long exposures 16 times per second. At the beginning of each second, one interruption is skipped, enabling the absolute time of each interruption to be determined with the help of the radiometer. The radiometer measures the total brightness of the sky with the frequency of 5000 Hz. The data are absolutely timed. Radiometers therefore provide both absolute time and detailed fireball light curves. Radiometric light curves are calibrated using photographic light curves, where fireball magnitudes can be determined by comparison with stars.

Table 1: Selected meteoroid parameters derived from the fragmentation model

No.	Fireball code	Mass	Density	Size	$p_1$	$p_{90\%}$	$p_{\max}$	Fraction		
		kg	kg m <sup>-3</sup>	cm	MPa	MPa	MPa	Abla.	Ero.	Dust
01	EN251015_022301	0.165	1000.	3.4	0.008	0.025	0.063	0.016	0.51	0.47
02	EN311015_180520	650.	500.	67.7	0.002	0.012	0.19	0.001	0.98	0.02
03	EN311015_231302	31.	1400.	17.4	0.009	0.051	0.19	0.003	0.95	0.05
04	EN011115_013625	0.015	1000.	1.5	0.070	0.085	0.17	0.17	0.00	0.83
05	EN021115_022525	0.23	500.	4.8	0.020	0.044	0.079	0.023	0.80	0.17
06	EN021115_232112	0.016	2000.	1.3	0.16	0.40	0.40	0.60	0.00	0.40
07	EN041115_021111	0.55	1500.	4.4	0.015	0.051	0.20	0.013	0.91	0.08
08	EN041115_203853	0.255	1000.	3.9	0.004	0.044	0.13	0.09	0.66	0.25
09	EN051115_023102	0.009	1000.	1.3	0.046	0.100	0.16	0.31	0.40	0.29
10	EN061115_040629	0.011	500.	1.7	0.001	0.045	0.075	0.26	0.30	0.44
11	EN081115_181258	0.050	200.	3.9	0.005	0.031	0.073	0.18	0.41	0.41
12	EN101115_235401	0.085	600.	3.2	0.016	0.047	0.083	0.04	0.48	0.48
13	EN131115_002058	0.008	250.	1.9	0.008	0.057	0.057	0.14	0.24	0.62
14	EN161115_193458	0.008	600.	1.5	0.011	0.132	0.15	0.57	0.13	0.30
15	EN161115_213048	0.018	1000.	1.6	0.031	0.059	0.080	0.08	0.23	0.69
16	EN281118_034715	1.5	250.	11.3	0.005	0.035	0.097	0.06	0.65	0.29
<i>nT</i>	<i>EN270217_023122</i>	<i>3.3</i>	<i>3400.</i>	<i>6.1</i>	<i>0.11</i>	<i>2.8</i>	<i>3.5</i>	<i>0.57</i>	<i>0.26</i>	<i>0.17</i>

## 2.2. Data

For the fragmentation analysis, 15 fireballs from the sample studied by Spurný et al. (2017) were selected. The sample was supplemented by the brightest Taurid fireball observed in 2018, EN 28118\_034715. The sample covers all fireball types from I to IIIB. Figure 1, modified from Spurný et al. (2017), shows the PE coefficient as a function of meteoroid mass. The masses of the analyzed meteoroids ranged from 8 grams to 650 kg. The fact that larger meteoroids are more fragile is clearly visible in Fig. 1.

Figure 2 shows the orbits of the modeled fireballs. There is no doubt that all 16 fireballs were members of the Taurid shower. The fireball list is provided in Table 1. Fireball no. 14 was a regular Southern Taurid; other Taurids belonged to the new branch. For the comparison of physical properties, we also included one non-Taurid, EN 270217\_023122, observed in February 2017, which had similar semimajor axis and eccentricity as Taurids and its entry speed (31 km s<sup>-1</sup>) was within the Taurid range (25 – 33 km s<sup>-1</sup>). The meteoroid physical properties were, however, very different, as it is shown in Table 1 and will be discussed later.

Figures 3–5 shows images and light curves of three Taurids of various brightness. The brightest observed fireball no. 2 had nearly symmetrical light curve and the maximal brightness of  $-18$  mag was reached already at a height of 81 km. There were also several short flares toward the end of the fireball. The radiometric light curve contains also the radiation of the stationary trail, which was very bright and formed around the position of the bolide maximum. The photographic light curve describes only the moving meteor. The medium brightness fireball no. 5 was characterized by a sudden increase of brightness by 4 magnitudes (i.e. nearly  $40\times$ ) in the second half of the trajectory (at a height 78 km), which formed the beginning of a broad flare. Fireball no. 6 was relatively faint, except two short flares. This fireball penetrated deeper than the previous two, down the height of 48 km (the end height was 54 km for fireball no. 2 and 65 km for fireball no. 5).

### 2.3. Modeling

The observed light curves and decelerations of fireballs were fitted by the semi-empirical fragmentation model. The model was described in detail in Borovička et al. (2013) and Popova et al. (2019). Short flares were modeled by an immediate release of dust, i.e. large number of small fragments, as it is illustrated in Fig. 6. Longer flares were modeled with the help of the formalism of eroding fragments (Fig. 7). Eroding fragments are releasing dust from their surfaces over prolonged period of time. The rate of mass loss in form of solid fragments is described by the erosion coefficient, analogous to the ablation coefficient (which describes the mass lost due to evaporation). A step-wise increase of brightness was modeled by fragmentation into a number of macroscopic regular (non-eroding) fragments (Fig. 6). Usually, all fragments were assumed to have the same mass for simplicity.

The main parameters of the model were the initial mass and density of the meteoroid, the heights of fragmentations, the mass of released dust, erosion fragments, and regular fragments at each fragmentation, the masses of dust grains, the densities of fragments, and the erosion coefficients. The fixed parameters were the intrinsic ablation coefficient  $0.005 \text{ s}^2\text{km}^{-2}$  (see Ceplecha and ReVelle, 2005), the product of drag and shape coefficients,  $\Gamma A = 0.8$ , dust grain density  $2000 \text{ kg m}^{-3}$ , and the luminous efficiency dependent on velocity and mass in the same way as for the Košice meteoroid (Borovička et al., 2013).

We are mostly interested in the heights of fragmentations, which together with the known velocity at that point,  $v$ , define the dynamic pressure  $p = \rho v^2$ .

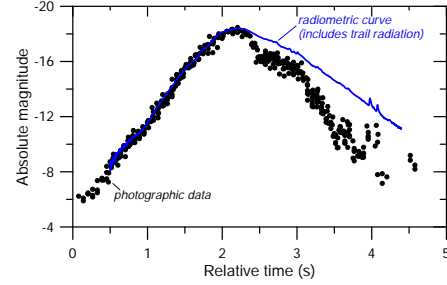


Figure 3: Image and light curve of Taurid fireball no. 2 (EN 311015\_180520). Dots are photographic data (from eight different cameras), the curve is from a radiometer.

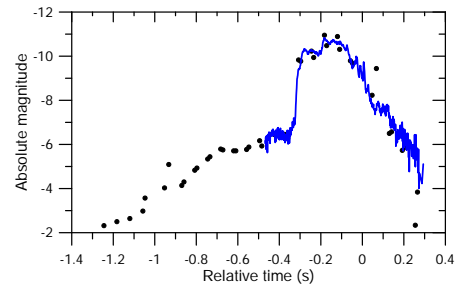


Figure 4: Image and light curve of Taurid fireball no. 5 (EN 021115\_022525). Dots are photographic data (from two different cameras), the curve is from a radiometer.

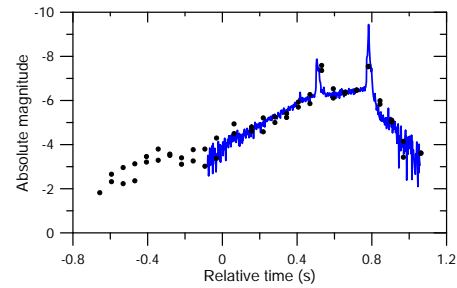


Figure 5: Image and light curve of Taurid fireball no. 6 (EN 021115\_232112). Dots are photographic data (from two different cameras), the curve is from a radiometer.

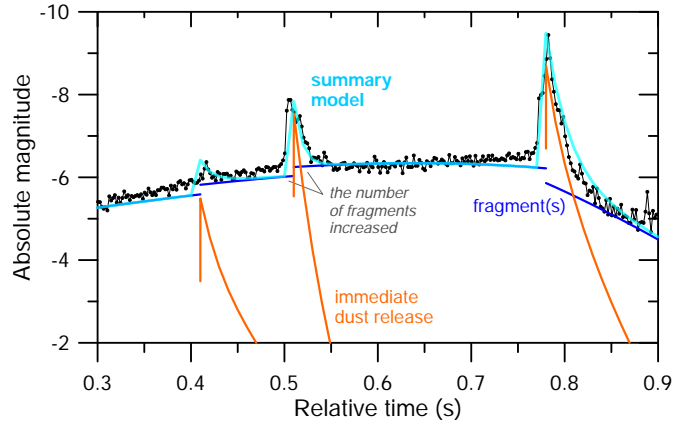


Figure 6: Fit of the light curve of Taurid fireball no. 6 demonstrating the explanation of short flares by immediate dust releases.

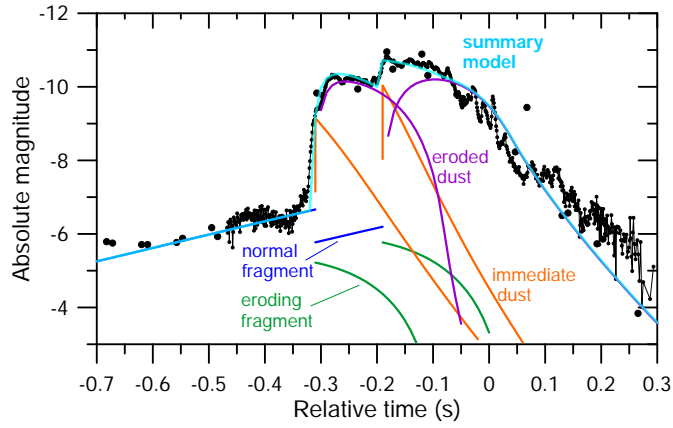


Figure 7: Fit of the light curve of Taurid fireball no. 5 demonstrating the dominating role of eroded dust in explanation of long flares.



The atmospheric density  $\rho$  was taken from the NRLMSISE-00 model (Picone et al., 2002). We define that the dynamic pressure is equal to the strength of the meteoroid, namely the strength of the part which was lost. The lost part is defined as the mass before fragmentation minus the mass of the largest regular fragment after fragmentation. Since multiple fragmentations were observed in all fireballs, strength distribution within the meteoroids could be studied. The heights of the fragmentations were quite obvious from the positions of flares on the light curve. The mass analysis is more model-dependent but the amplitudes and durations of flares are good indicators of the amount of lost mass.

Another parameter of interest is the meteoroid bulk density. It was primarily determined from the fireball brightness before the first fragmentation. If the meteoroid mass is known (basically from the total radiated energy) and the ablation coefficient and  $\Gamma A$  are fixed, the brightness of the fireball, when it is still single body and the ablation reached its steady-state, depends on meteoroid density. Lower density means larger cross section and larger brightness. In some cases, low density derived this way was confirmed by high deceleration. However, the used  $\Gamma A = 0.8$  assumes nearly spherical meteoroids. If a meteoroid was highly non-spherical, the derived density will be not valid. We must therefore consider the individually derived densities as rather uncertain. Note also that since the grain density was assumed to be  $2000 \text{ kg m}^{-3}$  (for presumably carbonaceous material), the highest possible meteoroid density was also  $2000 \text{ kg m}^{-3}$ .

### 3. Results

The list of modeled fireballs and some results of the model are given in Table 1. Note that the mass of the largest meteoroid (650 kg) is lower than 1300 kg given in Spurný et al. (2017) since only the radiation of the moving fragments was modeled. The radiation of the stationary trail, which was very intense in this case, cannot be explained by the fragmentation model and does not therefore enter to the energy budget.

Apart from the trail, the fragmentation model was able to explain the light curves and decelerations of Taurid fireballs almost perfectly. The only general problem seems to be terminal flares. Three fireballs (nos. 11, 12, and 15) exhibited bright terminal flares while the brightness before the flare was low and the deceleration also suggested meteoroid mass too low to produce the flare. The discrepancy could be solved by adjusting some parameters

(ablation coefficient,  $\Gamma A$ , or luminous efficiency) differently for the end of the fireball. The derived dynamic pressures at fragmentations were not affected by this problem.

For fireball no. 9, there was a problem to explain the increased deceleration after the first fragmentation at the height of 72 km. Since the brightness after the flare did not increase in comparison with the situation before the flare, the deceleration could not be explained by a disruption into small fragments. We had to assume that the velocity suddenly decreased by  $0.4 \text{ km s}^{-1}$  at the fragmentation. This was the only fragmentation event in our sample where a velocity change was introduced.

Deceleration was observed for all fireballs except no. 3, which was big and disintegrated quickly without leaving any observable fragments, which could be decelerated at lower heights. For most fireballs, the velocity at the end was  $5 - 10 \text{ km s}^{-1}$  lower than at the beginning. In some cases, the velocity decreased significantly only after the last fragmentation, in some cases it was decreasing along almost the whole trajectory. Fireballs nos. 1, 7, and 12 showed only minor decelerations with velocity difference less than  $2 \text{ km s}^{-1}$ . On the other hand, fireball no. 6 decelerated from 32 to  $12 \text{ km s}^{-1}$ . All these data were taken into account during the modeling.

### 3.1. Modes of mass loss

Figure 8 shows the fraction of mass lost by regular ablation (i.e. evaporation from macroscopic fragments, not dust), by erosion (i.e. in the form of dust from eroding fragments), and by suddenly released dust. There is a clear trend with mass. Erosion was the dominant process for all Taurid meteoroids larger than 0.1 kg. For smaller meteoroids, immediate dust release was increasingly important. Moreover, for two small meteoroids, ablation was the dominant process amounting for  $\sim 60\%$  of lost mass (see also Table 1). Any kind of fragmentation was therefore not so important for them. The non-Taurid did not follow the trend. Although having more than 3 kg, most mass was lost by regular ablation.

The masses of dust particles, both immediately released and eroded, ranged from  $10^{-12} \text{ kg}$  to  $5 \times 10^{-6} \text{ kg}$ . It corresponds, for the assumed density of  $2000 \text{ kg m}^{-3}$ , to sizes from about  $10 \text{ }\mu\text{m}$  to  $1.5 \text{ mm}$ . Meteoroids no. 3 and 6 contained only grains  $\geq 100 \text{ }\mu\text{m}$ . The opposite case was meteoroid no. 12, which contained only grains  $\leq 100 \text{ }\mu\text{m}$ . The typical size range for other meteoroids was  $20 - 500 \text{ }\mu\text{m}$ .

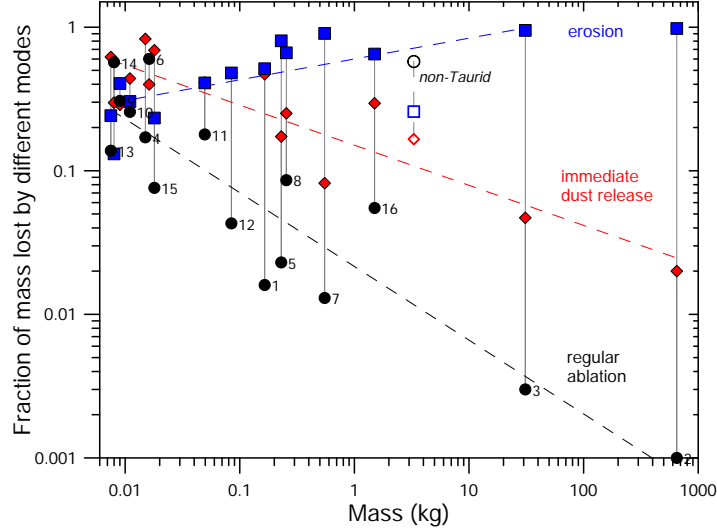


Figure 8: Part of the meteoroid mass lost by regular ablation of macroscopic fragments (black circles), immediate release of dust (red diamonds), and dust released gradually from eroding fragments (blue squares) as a function of initial mass. For meteoroid numbers see Table 1. The same data for the non-Taurid meteoroid are also shown (empty symbols).

### 3.2. Dynamic pressures

Figure 9 shows the mass loss of individual meteoroids as a function of increasing dynamic pressure during the atmospheric entry. Many meteoroids were subject to numerous fragmentation events. They demonstrated themselves by multiple flares on the light curve. Although the largest meteoroid no. 2 exhibited one very wide and bright flare, it was to be modeled by subsequent release of five eroding fragments. On the other hand, in some cases, e.g. meteoroids no. 5 and 6, there were only few (2–3) fragmentations.

All Taurids were much weaker than the non-Taurid meteoroid. The non-Taurid reached dynamic pressures up to 3 MPa. All Taurids except one were destroyed before they reached 0.2 MPa. In fact, parts of only three Taurids approached pressures of about 0.15 MPa. The largest of them was a 0.5 kg fragment of the  $\sim 30$  kg meteoroid no. 3. About 20 g (only 0.003% of the initial mass) remained from the huge meteoroid no. 2. But the small meteoroid no. 6 (14 g at that time) only started to fragment at this pressure. Two parts of it, both of about 2 grams, survived almost to 0.4 MPa.

Figure 10 shows the same data as Fig. 9 but the fragment mass is plotted in relative scale as a fraction of the initial mass. It is noticeable that many

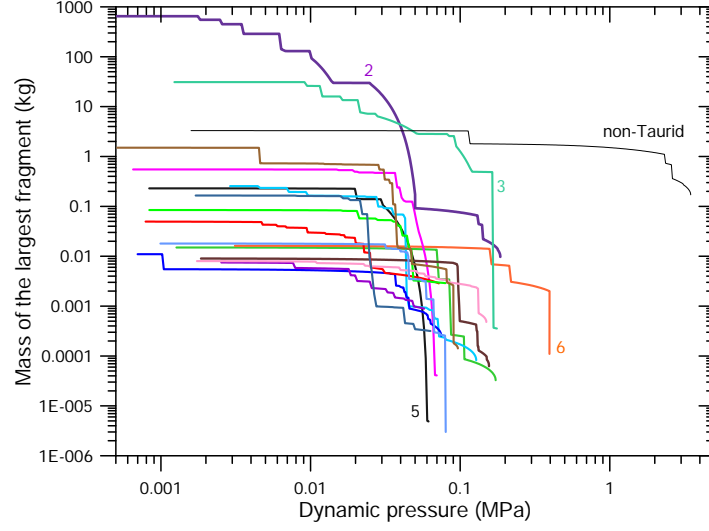


Figure 9: Mass of the largest surviving fragment as a function of increased dynamic pressure for 16 Taurids and one non-Taurid. Selected Taurids are identified by their numbers. For color legend see Fig. 10.

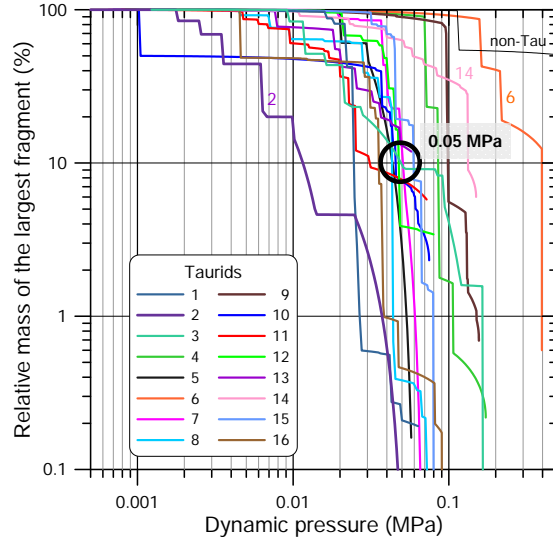


Figure 10: The same as Fig. 9 but with mass in relative scale.

Taurid meteoroids reached the level of 10% at nearly the same pressure of about 0.05 MPa. We therefore define the pressure  $p_{90\%}$  as the dynamic pressure when the meteoroid lost 90% of its initial mass. It was in the range 0.04–0.06 MPa for 8 Taurids and within 0.025–0.1 MPa for 13 of the 16 Taurids. It therefore seems that a characteristic property of most Taurids is that 90% of mass is lost, within a factor of two, at a pressure of 0.05 MPa. The obviously deviating case was the huge meteoroid no. 2 with  $p_{90\%} \sim 0.01$  MPa. At 0.05 MPa more than 99.9% of mass was lost. The opposite cases were small meteoroids no. 6 and 14 with  $p_{90\%}$  0.4 MPa and 0.13 MPa, respectively.

Figure 11 shows the characteristic pressures  $p_1$ ,  $p_{90\%}$ , and  $p_{\max}$  as a function of meteoroid mass. Here  $p_1$  is the pressure of first fragmentation and  $p_{\max}$  is the maximal reached pressure. The values are also listed in Table 1. Figure 11 shows also the median values of the pressures. For the first fragmentation, the median is 0.01 MPa, but there is very large scatter of the actual values. Meteoroid no. 10 broke up already at 0.001 MPa, although it was a rather quiet splitting into two similarly sized fragments and the next fragmentation (probably of the smaller of the two fragments) occurred at 0.01 MPa. The huge meteoroid no. 2 suffered complete disintegration between 0.0016 – 0.01 MPa. On the other hand, some small meteoroids were much stronger. As mentioned above, meteoroid no. 6 did not break up until 0.16 MPa.

The values of  $p_{90\%}$ , with median of 0.05 MPa, were already discussed. The median value of  $p_{\max}$  is 0.09 MPa. For almost all Taurids including the largest one, maximum pressure was within a factor of two of this median. The only exception was the strongest Taurid no. 6 with  $p_{\max} = 0.4$  MPa. But the non-Taurid was even much stronger with  $p_{\max} = 3.5$  MPa.

There is a weak trend of decrease of  $p_1$  and  $p_{90\%}$  with increasing meteoroid mass. Formally, it can be fitted by power index of about  $-0.16$ . But there is huge scatter of individual values. Except for the largest meteoroid no. 2, the power law function does not provide better prediction than using the median value.

There is no trend for  $p_{\max}$ . Maximal pressure was usually reached at the last fragmentation point. It therefore expresses the strength of the strongest macroscopic material contained in the meteoroid. Except for meteoroid no. 6, the strongest material seems to be nearly the same, irrespective of the initial meteoroid size. In four cases (fireballs nos. 4, 8, 10, and 14), the maximal pressure was reached shortly after the last fragmentation, when the largest surviving fragment was decelerated. In these cases, the maximal pressure

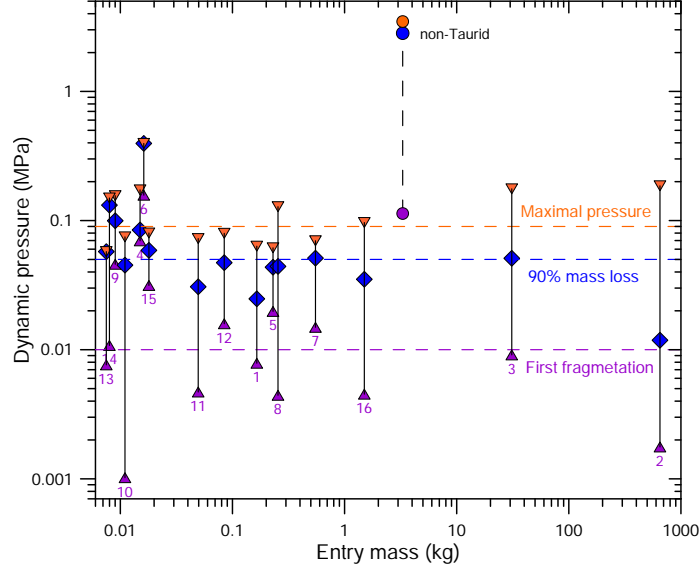


Figure 11: The dynamic pressure at the first fragmentation, at the time when 90% of mass was lost (i.e. the mass of the largest fragment decreased to 10% of the initial mass), and the maximal reached dynamic pressure as a function of initial mass. For meteoroid numbers see Table 1. Median values are shown as horizontal dashed lines. The values for the non-Taurid are plotted for comparison.

expresses just the lower limit of the strength of the last fragment. But all these fragments were small, with masses of 0.1 – 0.7 g.

### 3.3. Strength distribution

Since the model provided the dynamic pressure and the amount of mass lost for each fragmentation, we can study the strength distribution inside the meteoroids. The strength of the lost mass is considered to be equal to the dynamic pressure, at which it was lost. The statistics of strength was created for all 16 Taurids. The mass lost by ablation was ignored in the statistics.

We used the color codes presented in Fig. 12 to display the derived strengths graphically. The lowest strengths are in yellow and orange, the highest in green and dark blue. If the mass was lost by splitting into small number of similarly sized regular fragments rather than dust, eroding fragment or large number of small fragments, the color is hatched.

The results are presented in Fig. 13. It can be seen that the largest meteoroid no. 2 had very low strength. Only tiny fraction, hardly visible in Fig. 13, had strength larger than 0.02 MPa. Material of strength higher than

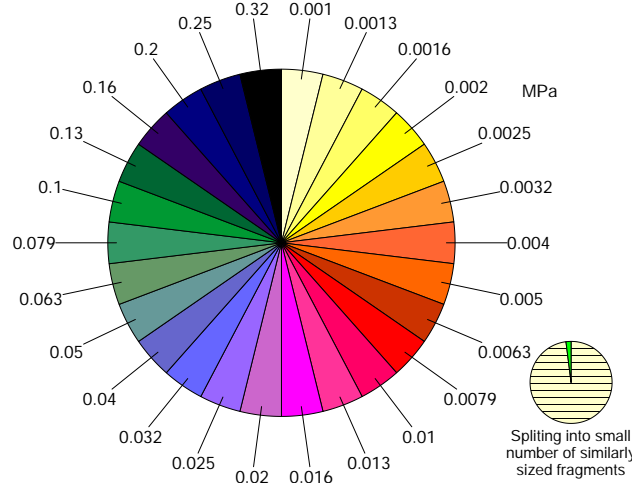


Figure 12: Color coding of strengths in the pie charts in Fig. 13. The color scale is logarithmic. Three steps correspond to the increase of strength two times.

0.1 MPa represented  $< 0.01\%$  of the mass and is invisible in the plot. The second largest meteoroid no. 3 was considerably stronger. Its weakest part was as strong as the strongest 5% of meteoroid no. 2. It also contained  $\sim 5\%$  of material stronger than 0.08 MPa and 1.5% stronger than 0.1 MPa. If we do not count splitting into similar pieces, smaller meteoroids rarely contained the very weak material which formed 95% of meteoroid no. 2. Some medium-sized meteoroids like nos. 8 and 11 were very heterogeneous and contained the very weak material in small amounts. Other medium-sized meteoroids like nos. 1, 5, and 7 were more homogeneous and contained mostly material of medium strength of 0.02–0.03 MPa. The smallest meteoroids nos. 4, 9, 14, 15 were composed mostly from stronger material of strengths of 0.05–0.1 MPa; no. 6 even 0.15–0.4 MPa.

Figure 14 shows the histogram of fragmentation pressures. The largest number of fragmentation events occurred at a pressure of about 0.04 MPa. Note that in contrast to Figs. 9 and 13, all modeled fragmentations, not only those of the largest surviving fragment, are considered in Fig. 14. From 174 total fragmentations, 159, i.e. more than 90%, occurred at pressures 0.01–0.2 MPa. This statistics, however, does not consider how representative individual fragmentations were, i.e. how large amount of mass was lost. The distribution considering the lost mass is shown in Fig. 15. Here the statistics is dominated by the four first fragmentations of the largest meteoroid no.

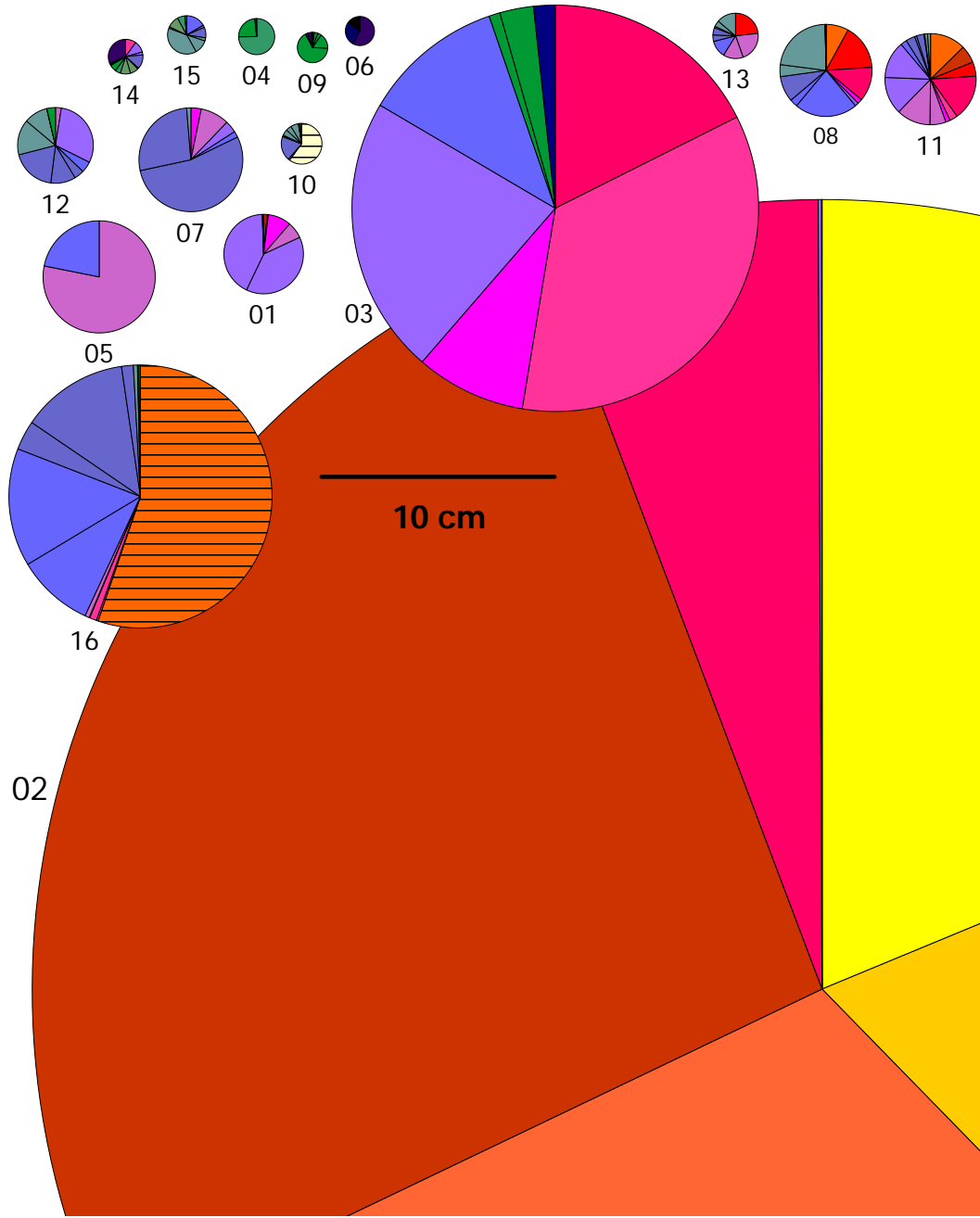


Figure 13: Distribution of strength in 16 Taurid meteoroids. For color code see Fig. 12. Individual meteoroids are represented by circles proportional to the meteoroid size (computed from the initial mass and density) and labeled by the numbers from Table 1. The plotted fractions are fractions of released mass.



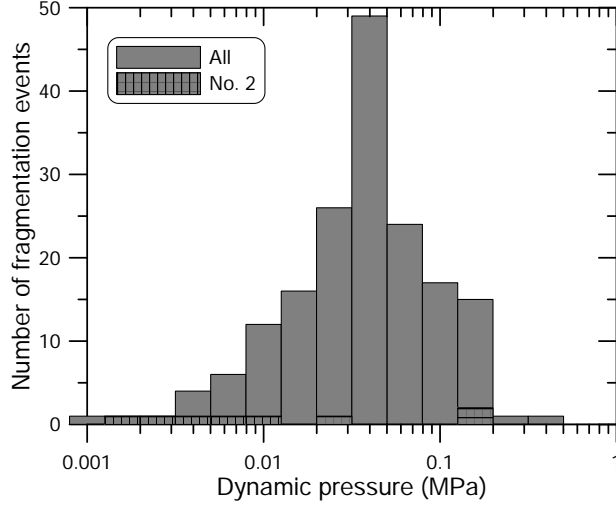


Figure 14: Number of all fragmentation events for all 16 Taurids as a function of dynamic pressure. Fragmentations of the largest meteoroid no. 2 are highlighted.

2, which all occurred at pressures  $< 0.01$  MPa and released huge amount of mass. If we therefore consider the Taurid material as a whole, the large majority had strengths  $0.0015\text{--}0.008$  MPa. This strength is much lower than the tensile strength of snow, which is about  $0.01 - 0.04$  MPa (Upadhyay et al., 2007). The amount of stronger material decreased nearly exponentially with increasing strength (Fig. 15b).

### 3.4. Bulk densities

Bulk densities of the incoming meteoroids are much more difficult to derive than fragmentation strengths. As explained in Section 2.3, the derived densities may be affected by unknown shapes of the meteoroids. The computed densities are listed in Table 1 and cover wide range from  $200$  to  $2000$   $\text{kg m}^{-3}$ . The strongest meteoroid no. 6 had the highest density, but otherwise no clear correlation with strength was found. There is only a weak correlation between the dynamic pressure at the first fragmentation,  $p_1$  (which can be called bulk strength), and bulk density (Fig. 16). The density of the weakest and largest meteoroid no. 2 was estimated to  $500$   $\text{kg m}^{-3}$  but the uncertainty is large in this case since steady-state ablation was not reached before the start of fragmentation. Note that the density of comet 2P/Encke was found to be rather uncertain  $800 \pm 800$   $\text{kg m}^{-3}$  (Sosa and Fernández, 2009). The

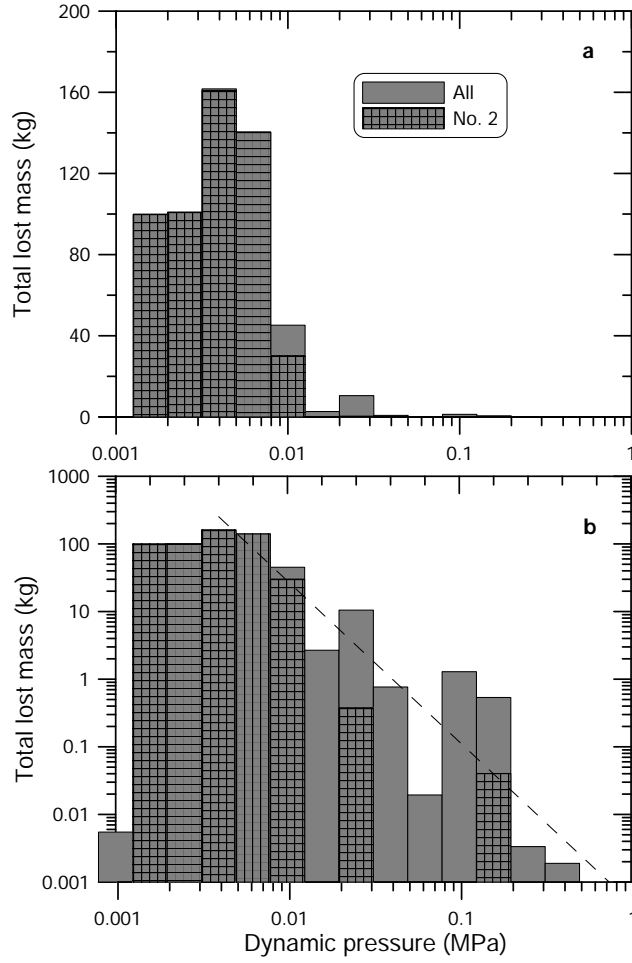


Figure 15: Total mass lost in all fragmentation events for all 16 Taurids as a function of dynamic pressure. Fragmentations of the largest meteoroid no. 2 are highlighted. The same data are shown in linear (a) and logarithmic (b) scale.

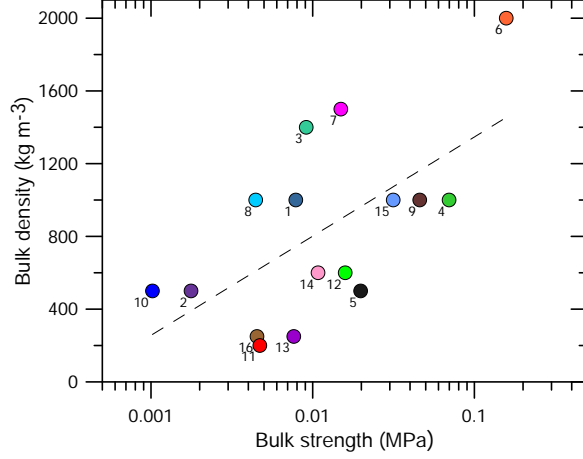


Figure 16: Bulk densities of Taurid meteoroids as a function of dynamic pressure at the first fragmentation. For fireball numbers see Table 1.

mean value for all comets studied so far is  $480 \pm 220 \text{ kg m}^{-3}$  (Groussin et al., 2019).

#### 4. Discussion and conclusions

We provided the most detailed study so far of the material properties of Taurid meteoroids. It was important that we had a compact orbital sample and there was no doubt that all studied meteoroids belonged to the Taurid stream. Most of them belonged to the resonant swarm, which, in fact, could be described in detail thanks to the quality of our orbital data (Spurný et al., 2017).

This study was based on the modeling of atmospheric fragmentation of meteoroids. The availability of precise radiometric light curves with high temporal resolution was crucial for the modeling. It was also very important that our sample contained the extremely bright ( $-18$  mag) Taurid fireball EN 311015\_180520, which was caused by a meteoroid approaching size of one meter. One of main results of our study is that large Taurid meteoroids have different properties than smaller ones (cm-sized). Note that Taurid stream is unique among all meteoroid streams in containing very large meteoroids (Brown et al., 2013). We believe that EN 311015\_180520 was not exceptional and its properties are typical for Taurids of similar sizes. As mentioned in

Spurný et al. (2017), all probable Taurid superbolides detected by the US Government Sensors reached their maxima at very high altitudes.

Our analysis showed that when taking the Taurid material as a whole, the majority has very low strength of  $< 0.01$  MPa. Such low strength material exists mostly as large bodies ( $\gg 10$  cm), can form a significant part of medium-sized bodies ( $\sim 10$  cm), and only rarely is encountered in smaller bodies, where it forms a minority. Stronger materials exist in Taurids as well, but their occurrence decreases exponentially with strength. Strong material forms small inclusions in large bodies or exists as small (cm-sized) separate bodies. A typical not too large Taurid lose 90% of its mass when the dynamic pressure reaches 0.05 MPa. All these properties suggest that it is unlikely that Taurids can produce meteorites. The material, which could potentially be strong enough to survive the atmospheric passage, is too small.

Taurid properties strongly suggest their cometary origin. Low strength and low density (likely  $< 1000$  kg m<sup>-3</sup> for most material) is typical for comets. Even the asteroids such as 2015 TX24 that are part of the Taurid new branch (Spurný et al., 2017) are likely of cometary origin. The existence of large fragile bodies within the stream suggest a quiet process of comet disintegration. Some of these large bodies may have collided with the Earth in the past and some may do it in the future. The grand comet hypothesis (Clube and Napier, 1984) seems to be plausible.

#### *Acknowledgments*

This work was supported by grant no. 19-26232X from the Czech Science Foundation. The observations by DAFO were made possible thanks to the Praemium Academiae from the Czech Academy of Sciences. The institutional project was RVO:67985815.

#### **References**

- Asher, D. J., Clube, S. V. M., 1993. An extraterrestrial influence during the current glacial-interglacial. *Quart. J. Roy. Astron. Soc.* 34, 481-511.
- Babadzhanov, P. B., Kokhirova, G. I., 2009. Densities and porosities of meteoroids. *Astron. Astrophys.* 495, 353–358.
- Bellot Rubio, L. R., Martínez González, M. J., Ruiz Herrera, L., Licandro, J., Martínez-Delgado, D., Rodríguez-Gil, P., Serra-Ricart, M. 2002. Modeling

- the photometric and dynamical behavior of Super-Schmidt meteors in the Earth's atmosphere. *Astron. Astrophys.* 389, 680-691.
- Borovička, J., Tóth, J., Igaz, A., Spurný, P., Kalenda, P., Haloda, J., Svoreň, J.; Kornoš, L., Silber, E., Brown, P., Husárik, M., 2013. The Košice meteorite fall: Atmospheric trajectory, fragmentation, and orbit, *Meteoritics and Planetary Science*, 48, 1757–1779.
- Brown, P., Marchenko, V., Moser, D. E., Weryk, R., Cooke, W., 2013. Meteorites from meteor showers: A case study of the Taurids. *Meteoritics and Planetary Science* 48, 270-288.
- Ceplecha, Z., McCrosky, R. E., 1976. Fireball end heights - A diagnostic for the structure of meteoric material. *J. Geophys. Res.* 81, 6257-6275.
- Ceplecha, Z., Revelle, D. O., 2005. Fragmentation model of meteoroid motion, mass loss, and radiation in the atmosphere, *Meteoritics and Planetary Science*, 40, 35-50.
- Clube, S. V. M., Napier, W. M., 1984. The microstructure of terrestrial catastrophism. *Mon. Not. Roy. Astron. Soc.* 211, 953-968.
- Groussin, O., Attree, N., Brouet, Y., Ciarletti, V., Davidsson, B., Filacchione, G., Fischer, H.-H., Gundlach, B., Knapmeyer, M., Knollenberg, J., Kokotanekova, R., Kührt, E., Leyrat, C., Marshall, D., Pelivan, I., Skorov, Y., Snodgrass, C., Spohn, T., Tosi, F. 2019. The thermal, mechanical, structural, and dielectric properties of cometary nuclei after Rosetta. *Space Science Reviews* 215:29.
- Jenniskens, P., 2006, *Meteor Showers and their Parent Comets*. Cambridge Univ. Press
- Kasuga, T., Jewitt, D., 2019. Asteroid-meteoroid complexes. In *Meteoroids: Sources of Meteors on Earth and Beyond*, Ryabova G. O., Asher D. J., and Campbell-Brown M. D. (eds.), Cambridge, UK, Cambridge University Press, 336 pp., p. 187-209.
- Konovalova, N. A., 2003. Interaction of large Taurid meteoroids with the Earth's atmosphere. *Astron. Astrophys.* 404, 1145-1152.

- Madiedo, J. M., Ortiz, J. L., Trigo-Rodríguez, J. M., Dergham, J., Castro-Tirado, A. J., Cabrera-Caño, J., Pujols, P., 2014. Analysis of bright Taurid fireballs and their ability to produce meteorites. *Icarus* 231, 356-364.
- Matlovič, P., Tóth, J., Rudawska, R., Kornoš, L., 2017. Spectra and physical properties of Taurid meteoroids. *Planetary and Space Science* 143, 104-115.
- Picone, J. M., Hedin, A. E., Drob, D. P., Aikin, A. C., 2002. NRLMSISE-00 empirical model of the atmosphere: Statistical comparisons and scientific issues. *J. Geophys. Res. (Space Physics)* 107 (A12), 1468.
- Popova, O., Borovička, J., Campbell-Brown, M. D. , 2019. Modelling the entry of meteoroids. In *Meteoroids: Sources of Meteors on Earth and Beyond*, Ryabova G. O., Asher D. J., and Campbell-Brown M. D. (eds.), Cambridge, UK, Cambridge University Press, 336 pp., p. 9-36.
- Sosa, A., Fernández, J. A. 2009. Cometary masses derived from non-gravitational forces. *Mon. Not. Roy. Astron. Soc.* 393, 192-214.
- Spurný, P., Borovička, J., Mucke, H., Svoreň, J., 2017. Discovery of a new branch of the Taurid meteoroid stream as a real source of potentially hazardous bodies. *Astron. Astrophys.* 605, A68.
- Spurný, P., Borovička, J., 2019. Activity of the new branch of resonant Taurids unexpectedly observed by the European Fireball Network in 2018. Presented at *Meteoroids 2019* (poster #8).
- Upadhyay, A., Joshi, S. K., Chandel, C., 2007. Tensile strength of snow using centrifugal technique. *Defence Science Journal* 57, 787-795.